INL/CON-17-43320-Revision-0

Deuterium Retention in Neutron-Irradiated Single-Crystal Tungsten

Masashi Shimada, Y. Oya, W. R. Wampler, Y. Yamauchi, C. N. Taylor, L. M. Garrison, L. M. Garrison, Y. Hatano

September 2017

The INL is a U.S. Department of Energy National Laboratory
operated by Battelle Energy Alliance

INL/CON-17-43320-Revision-0

Deuterium Retention in Neutron-Irradiated Single-Crystal Tungsten

Masashi Shimada, Y. Oya, W. R. Wampler, Y. Yamauchi, C. N. Taylor, L. M. Garrison, L. M. Garrison, Y. Hatano

September 2017

Idaho National Laboratory
Idaho Falls, Idaho 83415

http://www.inl.gov

Prepared for the
U.S. Department of Energy

Under DOE Idaho Operations Office
Contract DE-AC07-05ID14517

Accepted manuscript (FUSION_FUSENGDES-D-17-00840)

Deuterium Retention in Neutron-Irradiated Single-Crystal Tungsten

M. Shimada[*,a], Y. Oya[b], W.R. Wampler[c], Y. Yamauchi[d], C.N. Taylor[a], L.M. Garrison[e], D.A. Buchenauer[f], and Y. Hatano[g]

[a] *Idaho National Laboratory, Idaho Falls, ID, U.S.A.*
[b] *Shizuoka University, Shizuoka, Japan*
[c] *Sandia National Laboratories, Albuquerque, NM, U.S.A.*
[d] *Hokkaido University, Sapporo, Japan*
[e] *Oak Ridge National Laboratory, Oak Ridge, TN, U.S.A.*
[f] *Sandia National Laboratories, Livermore, CA, U.S.A.*
[g] *University of Toyama, Toyama, Japan*

Six single crystal tungsten specimens were neutron irradiated to a dose of 0.1 displacements per atom (dpa) at three different irradiation temperatures (633K, 963K, and 1073K) at the High Flux Isotope Reactor in Oak Ridge National Laboratory under the US-Japan PHENIX project. A pair of neutron-irradiated tungsten specimens was exposed to deuterium (D) plasma to D ion fluence of 5.0×10^{25} m^{-2} at three different exposure temperatures (673K, 873K, and 973K) at the Tritium Plasma Experiment in Idaho National Laboratory. A combination of thermal desorption spectroscopy, nuclear reaction analysis, and rate-diffusion modeling code (Tritium Migration Analysis Program, TMAP) were used to understand D behavior in neutron-irradiated tungsten. A broad D desorption spectrum from the plasma-exposure temperature up to 1173K was observed. Total D retention up to 1.9×10^{21} m^{-2} and near-surface D concentrations up to 1.7×10^{-3} D/W were experimentally measured from the 0.1 dpa neutron-irradiated single crystal tungsten. Trap density up to 2.0×10^{-3} Trap/W and detrapping energy ranging from 1.80 to 2.60 eV were obtained from the TMAP modeling.

Keywords: *tungsten, single crystal, plasma-facing components, plasma-material interaction, tritium retention, neutron-irradiation*

1. Introduction

Fusion promises to supply clean electricity with exceptional safety performance. The in-vessel tritium inventory source term (i.e. tritium retention) is one of the critical safety evaluation terms used in reactor safety assessments for licensing fusion facilities [1,2]. Minimizing tritium retention is a primary approach for fusion safety. 14 MeV neutrons produced by deuterium (D) – tritium (T) fusion reactions create radiation damage and defects in plasma-facing components (PFCs) and structural materials. These defects act as trapping sites for diffusing D and T atoms in materials, and there is a safety concern associated with the increased T retention in neutron-irradiated PFCs in the burning plasma environment. The neutron effects in tungsten, a leading candidate PFCs for DEMO, were identified as one of the critical research areas [3]. Improving the understanding of D/T behavior (i.e. retention and permeation) in neutron-irradiated tungsten is a key to achieving the safety goal.

D retention in neutron-irradiated polycrystalline tungsten was investigated for the first time under the previous US-Japan TITAN project [4-7]. Current US-Japan Technological Assessment of Plasma Facing Components for DEMO Reactors (PHENIX) project aims at understanding D/T behavior in neutron-irradiated tungsten and tungsten alloy at DEMO relevant elevated temperatures [8,9].

D retention studies from unirradiated, heavy-ion damaged, and self-ion damaged tungsten suggested that D retention would be negligibly small in damaged tungsten at elevated temperature (>773 K) [10]. One notable observation from the previous TITAN studies was that a large amount of D atoms were trapped in bulk tungsten at an elevated temperature of 773K, and D atoms had migrated to 10's of μm deep from the plasma-exposed surface even at relatively low D ion fluence of 1.0×10^{26} m^{-2} [7]. This discrepancy between ion-damaged and neutron-irradiated tungsten studies was mainly due to the damage distribution (e.g. near-surface damage (up to 2-3 μm) in ion-damaged vs. bulk damage (>> 100's μm) in neutron-damaged) and desorption of D atoms from near-surface traps during the plasma cool-down (ramp-down) phase. Hydrogen isotope diffusivity increases exponentially with temperature in metal. D/T atoms can migrate to the bulk (>> 100's μm) at elevated temperature, and can become trapped in the bulk PFCs materials. For the above reasons, accurately evaluating D retention at elevated temperature is challenging with near-surface ion-damaged tungsten specimens.

The objective of the PHENIX Task 3 is to investigate the safety concern of D/T retention in neutron-irradiated tungsten associated with operating at elevated temperature for DEMO, and try to understand the mechanism(s) of this deep diffusion and trapping of D/T atoms in neutron-irradiated tungsten at elevated temperature. In this work we report the progress on D retention research in neutron-irradiated single-crystal

*Corresponding author address: 2525 N. Fremont Ave., Idaho Falls, ID, 83415, U.S.A.
*Corresponding author E-mail: Masashi.Shimada@inl.gov

tungsten under PHENIX Task 3, with the experimental procedures for neutron-irradiation and plasma-exposure in Section 2, modeling method in Section 3, experimental results in Section 4, and modeling results in Section 5.

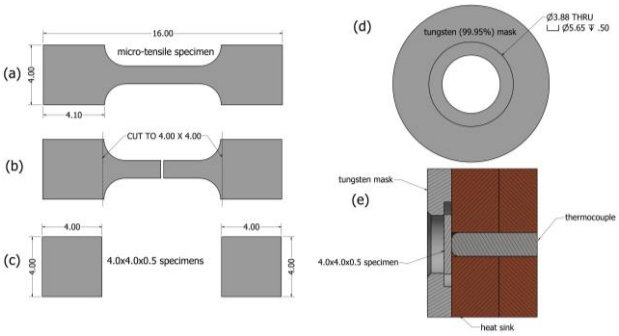

Figure 1: Schematic of specimen preparation (a-c) and specimen mounting configuration in TPE (d-e)

2. Experiment

2.1 Material Selection

Single crystal tungsten (SCW) specimens (Goodfellow USA, 99.999% purity) were originally prepared with electrical discharge machining, and polished with #800 grit polishing papers as micro-tensile specimens (4.0x4.0x16.0 mm^3) for tensile testing. The single crystal specimens were machined such that the <100> crystallographic direction was parallel to the tensile direction. The undeformed tab sections of the micro-tensile specimens were machined to 4.0x4.0x0.5 mm^3 size for this work as shown in Figure 1(a)-(c). The two undeformed tabs from three micro tensile testing specimens produced a total of six specimens, where each specimen had a nominally identical pair (A and B, respectively). The specimen ID numbers were labeled by argon ion beam milling on one sides of each specimen. The other smooth surface sides were used for plasma-exposure in this work. Heat treatment was not performed to remove surface damages from the mechanical polishing prior to neutron-irradiation. Before neutron irradiation, the surface was characterized by a grid of shallow cracks (artifacts from the electrical discharge machining) and parallel striations (artifacts from the #800 grit polish). The neutron irradiation and plasma exposure did not noticeably alter the surface state, so these same features were also present as shown in Figure 2. It is expected that the near surface region is composed of sub-grains from the mechanical polish while the bulk of the specimen is still a single crystal. These specimens do not have perfect mirror-finished conditions often used for laboratory experiments, but they represent realistic technical surfaces of the PFCs for future fusion reactors. The effects of rough or technical surfaces on D retention, surface morphologies and blister formation in tungsten were investigated, and reductions of D retention and blister formation near surface were reported in tungsten [11,12]. In this work the effect of technical surfaces on D retention is examined with an unirradiated single crystal tungsten specimen prepared in a similar procedure.

2.2 Neutron Irradiation

Neutron irradiation was performed in one of the central flux trap positions in the High Flux Isotope Reactor (HFIR) at Oak Ridge National Laboratory (ORNL). The micro-tensile tungsten specimens were irradiated at the HFIR in three different capsules (capsule ID: TB-300-2, TB-500-2, and TB-650-3) at three different irradiation temperatures (633K, 963K, and 1073K). The tungsten specimens were loaded inside molybdenum capsules with inert gas (helium and argon) filled conditions. Irradiation temperatures were determined by analyzing post-mortem SiC temperature sensors. Fast neutron fluence was (0.46-0.54) x 10^{25} n/m^2 (E > 0.1 MeV) for TB-300-2, TB-500-2, and TB-650-3 capsules. The radiation damage of approximately 0.1 displacements per atom (dpa) was calculated in the tungsten specimens by the SPECTER (neutron damage calculations for materials under irradiations) code with the neutron energy spectrum and fluence at the HFIR central flux trap position [13]. Highest neutron energy in HFIR is around 2-3 MeV and the He-4 production rate by neutron is negligibly low at < 3 MeV neutron energy.

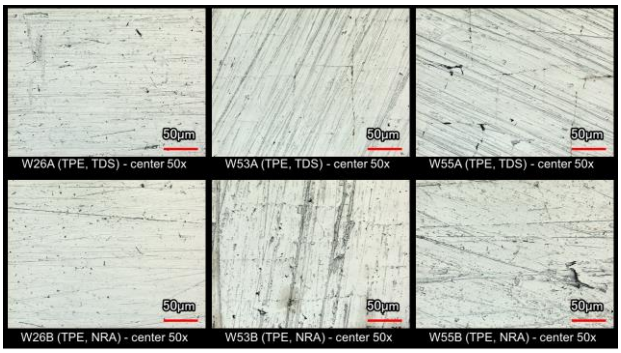

Figure 2: Microscope images on the plasma-exposed area in HFIR neutron-irradiated single-crystal tungsten specimens after TDS (A specimens) and NRA (B specimens)

2.3 Plasma Exposure

After sufficient cool-down time, the three capsules were opened at the ORNL's hot cell facility, and tensile testing was performed at ORNL. A total of six neutron-irradiated specimens (two 4.0x4.0x0.5 mm^3 specimens from the undeformed section of each micro-tensile specimen) were shipped to the Safety and Tritium Applied Research (STAR) facility in Idaho National Laboratory (INL). A 100% D plasma exposure was performed to <100> surface of SCW specimens with the Tritium Plasma Experiment (TPE), which is a high-flux linear plasma device capable of handling neutron-irradiated materials [14-16]. Table 1 shows the experimental conditions (HFIR irradiation and TPE plasma) used in this study. Incident ion energy was approximately 100 eV based on the biasing voltage of -100 V and typical plasma potential -5~0 V in the TPE plasma. A pure (99.95 %) tungsten mask with a inner

diameter of 3.88 mm was used to mount the specimens to the heat sinks, and a thermocouple (TC) was attached on the back of the specimen for specimen temperature measurement as shown as Figure 1(d)-(e). A pair (A and B) of neutron-irradiated tungsten specimens was exposed to D plasma to a similar D ion fluence of $5.0x10^{25}$ m^{-2} at 673K (400°C), 873K (600°C), and 973K (700°C). The A specimens (W53A, W55A, and W26A) were used for thermal desorption spectroscopy (TDS) study, and the B specimens (W53B, W55B, and W26B) were used for D-^{3}He nuclear reaction analysis (NRA) at Sandia National Laboratories – New Mexico. A 100% D plasma was used for both A and B specimens to obtain D depth profiling from the D-^{3}He NRA technique.

Table 1. The experimental (HFIR irradiation[a] and TPE plasma[b]) conditions.

Specimen ID	HFIR irradiation temp. [K]	TPE exposure temp. [K]	TPE exposure flux ($m^{-2}s^{-1}$)	TPE exposure fluence (m^{-2})
W53A	633	673	7.1E+21	5.1E+25
W53B	633	673	4.7E+21	5.0E+25
W55A	963	873	8.2E+21	5.2E+25
W55B	963	873	5.9E+21	5.0E+25
W26A	1073	973	8.4E+21	5.0E+25
W26B	1073	973	7.5E+21	5.0E+25

[a] HFIR irradiation dose was calculated to approximately 0.1 dpa based on the fast neutron fluence of (0.46-0.54)E+25 n/m^2 (E > 0.1 MeV).

[b] Incident ion energy was approximately 100 eV based on the biasing voltage of -100 V and typical plasma potential -5~0 V in TPE plasma.

2.4 Post Irradiation/Exposure Examination

The A specimens (W53A, W55A, and W26A) were transferred to the TDS system within 2-4 hours after the D plasma exposure in the TPE. Exposure to the air from the TPE vacuum chamber to the TDS vacuum chamber was unavoidable, but the exposure time to the air was typically kept less than 1 hr during the transfer. A specimen was loaded on a tantalum tray, and two TCs were in direct contact with the specimen front surface for temperature measurement. An infrared tube furnace (Research Inc. ChamberIR) was turned on only after the vacuum pressure reached below $1.0x10^{-5}$ Pa. Thermal desorption was performed with a ramp rate of 10K/min to 1173K and a temperature hold at 1173K for 0.5 hr. The tube furnace was turned off at the end of the 0.5 hr temperature hold. Details of the TDS system were reported elsewhere [7,14]. Three standard leaks provided an absolute D_2 sensitivity calibration for the residual gas analyzer (MKS Instrument e-Vision 2). A background desorption spectrum was established by heating a virgin specimen with a ramp rate of 10K/min to 1173K and a temperature hold at 1173K for 0.5 hr. Only the peaks associated with mass 3 (HD) and mass 4 (D_2) peaks were considered, and the same sensitivity was assumed for mass 3 and mass 4.

The B specimens (W53B, W55B, and W26B) were shipped to the Ion Beam Laboratory at Sandia National Laboratories – New Mexico approximately two weeks after the D plasma exposure. The D depth profiles within 3 μm from the plasma-exposed surfaces were measured by the D(^{3}He,p)α NRA technique with a 2.5 MeV ^{3}He ion beam within 30 days from the D plasma exposure. Energy spectra of the protons were measured using a large surface area (300 mm^2) and large depletion depth (1500 μm) annular-type silicon surface barrier detector mounted close to the specimen to obtain high solid angle and proton signal counts. A 12 μm thick Mylar foil was used to stop elastically scattered ^{3}He from reaching the detector. The D depth profiles were obtained by fitting the proton energy spectra with the SIMNRA code [17,18].

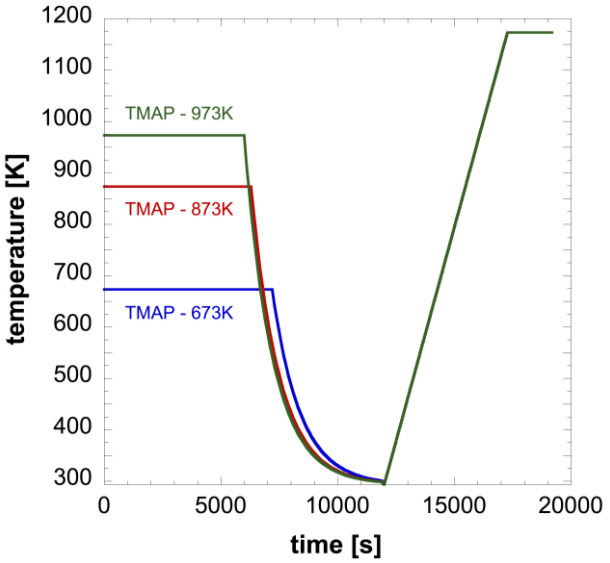

Figure 3: Temperature profiles used in the modeling for 673, 873, and 973K. The time constant of 1200 s was used to simulate the cool-down process after the TPE plasma exposure. Thermal desorption was simulated with the ramp rate (10 K/min) from 293K to 1173K and the temperature hold at 1173K for 0.5 hr from t=12000 s to 19190 s.

3. Modeling

A diffusion-reaction code, the Tritium Migration Analysis Program (TMAP) code, was developed by the Fusion Safety Program at INL in the 1980's for modeling T transport during normal and off-normal/accident conditions for fusion safety analysis. Recently the TMAP trap modeling capability was enhanced in the version 4 (TMAP4) to include as many traps as required by the user to simulate D/T behavior in neutron-irradiated tungsten [19-21]. The recently modified version of TMAP4 was used in this work.

For mass transport properties of D in tungsten, we chose the hydrogen diffusivity formula by Frauenfelder [22] (corrected for deuterium) as suggested in the review paper by Causey ($D_D=2.9x10^{-7}exp(-0.39eV/kT)$ [m^2/s]) in this work [23]. We assumed the surface D concentration to be zero as a boundary condition, $C_D(x=0)=0$, as suggested by Causey [23]. As a source term, the D implantation profile (100 eV D ion in tungsten) obtained from the SRIM code was fitted with a normal distribution [24]. The fitted normal distribution (with a center depth of $2.64x10^{-9}$ m and a half width at half maximum of $1.79x10^{-9}$ m) was used to simulate D ion implantation. The integrated fraction of D atoms in the

normal distribution (= 1 - reflection coefficient, R_{ref}) was adjusted as one of three fitting parameters to account for a complex plasma-surface interaction.

At high incident D flux and low temperature (i.e. low diffusivity) condition, the local concentration of D in solution within the implantation depth (2-4 nm) is high and the very high corresponding equilibrium gas pressure causes near-surface precipitation [25]. Interconnection of gas bubbles to the surface provides escaping paths for precipitated D_2, which reduces the diffusion length for release of D from solution. This increases the fraction of incident D released and decreases the concentration of D in solution available for diffusion beyond the implantation depth. The increased D release by this mechanism was included in the simulation by adjusting the reflection coefficient, R_{ref}. The detrapping energy, E_{det}, is defined as the sum of the binding energy of D atom in trapping site, E_{bin}, and the activation energy of D diffusion in tungsten, E_d, which is 0.39 eV [22]. The value of 10^{-13} s^{-1} was used as a pre-exponential factor for detrapping, and the trapping rate coefficient, α_{trap}, was defined as $\alpha_{trap} = D_D/\lambda_W$ where the lattice constant for tungsten, λ_W=3.16x10^{-10} m.

A single type of trapping site with a single detrapping energy was considered in this work, and uniform distribution of empty traps was introduced first. Uniform trap concentration throughout specimen thickness (0.5 mm) was assumed due to the unavailability of a D depth profile diagnostic in bulk W (> 3.0 μm). D plasma exposure was simulated from t=0 with the experimentally obtained D ion flux to investigate D behavior (e.g. how deep deuterium atoms migrate and become trapped) in tungsten. Figure 3 shows the temperature profiles used in the work for 673, 873, and 973K. Slightly different plasma exposure time was used to obtain the similar D ion fluence of 5.0x10^{25} m^{-2} with the different ion flux densities in W53A, W55A, and W26A. The time constant, T_{const}= 1200 s, was used to simulate the cool-down process after the TPE plasma exposure. Following the plasma-termination and the cool-down to room temperature (293K), thermal desorption was simulated with the ramp rate (10 K/min) from 293K to 1173K and the temperature hold at 1173K for 0.5 hr. The thermal desorption phase begins at t=12000 s and ends at 19190 s. We modeled the experiment (both D plasma exposure and thermal desorption) with three fitting parameters: 1) trap concentration, n_{trap} [Trap/W], 2) detrapping energy, E_{det} [eV], and 3) reflection coefficient, R_{ref}. We used the measured near-surface D concentration by NRA as a starting point for the trap concentration. In general, the first fitting parameter, trap concentration, can be obtained by the maximum deuterium flux (peak height) of TDS peak, and the second fitting parameter, detrapping energy, can be determined by the TDS peak positions. The third fitting parameter, reflection coefficient, R_{ref}, was also determined by the peak positions and maximum deuterium flux (peak height) of TDS spectrum.

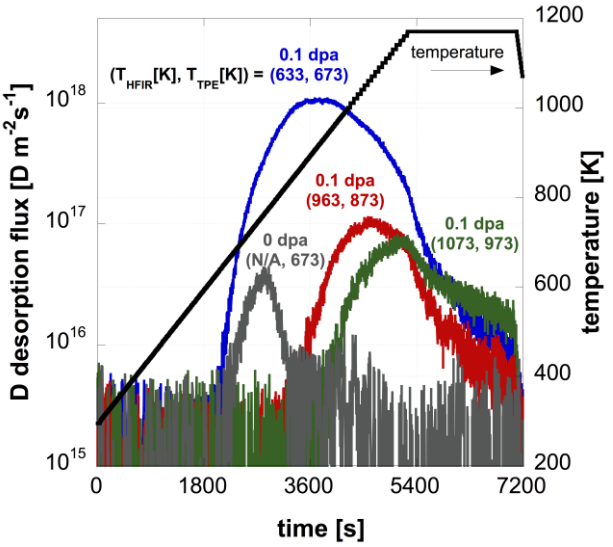

Figure 4: D desorption from A specimens (W53A, W55A, and W26A) exposed to D ion fluence of 5.0x10^{25} m^{-2} at 673K, 873K, and 973K, respectively. D desorption from the controlled (0 dpa) specimen exposed to D ion fluence of 5.0x10^{25} m^{-2} at 673K was shown as a comparison.

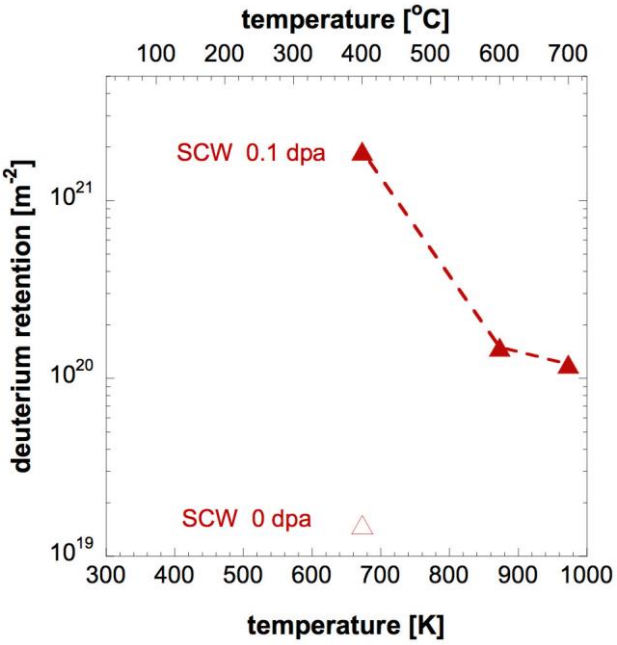

Figure 5: Total deuterium retention from 0.1 dpa neutron-irradiated single crystal tungsten SCW (in solid triangles) and unirradiated (0 dpa) single crystal tungsten SCW (in open triangle).

Table 2. The NRA and TDS result from 0.1 dpa HFIR neutron-irradiated tungsten specimens.

Specimen ID[a]	NRA[b] near-surface D conc. [D/W]	NRA[c] near-surface D retention [D m^{-2}]	TDS total D retention [D m^{-2}]	Ratio of TDS D retention to NRA D retention
W53A/B	1.7E-3	3.8E+20	1.9E+21	5
W55A/B	1.5E-4	8.7E+18	1.5E+20	17
W26A/B	4.9E-5	2.1E+18	1.2E+20	57

[a] The A specimens were used for TDS measurements and the B specimens were used for NRA measurements.
[b] NRA near-surface D concentration was the averaged D/W value from the depth of 2.5 to 3.0 μm.
[c] NRA near-surface D retention was the integrated D/W from 0.0 to 3.0 μm.

[d] TDS total D retention was the integrated D desorption flux from room temperature (at t=0 s) to the end of the 0.5 hr temperature hold (t~7200 s.)

4. Experimental Results

Figure 4 shows the D desorption fluxes from the A specimens (W53A, W55A, and W26A) exposed to D ion fluence of $5.0x10^{25}$ m^{-2} at 673K, 873K, and 973K. D desorption flux from an unirradiated (0 dpa) specimen exposed to D ion fluence of $5.0x10^{25}$ m^{-2} at 673K is shown as the grey line for comparison. In addition, the specimen temperature evolution is plotted as the black line. Note that the vertical y-axis (D desorption flux) is plotted in log scale. D desorption from the unirradiated (0 dpa) specimen showed a small sharp peak around 773K, and high-temperature desorption was not observed. Total D retention was approximately $1.5x10^{19}$ m^{-2} for the unirradiated (0 dpa, 673K) specimen. The D desorption spectrum was similar to unirradiated polycrystalline specimen exposed to a similar TPE plasma [7]. D desorption from specimen W53A (0.1 dpa, 673K) showed a broad desorption peak starting from 673K (plasma-exposure temperature) up to 1173K (maximum TDS temperature) with the peak temperature around 873K. The broad peak is characteristic of slow D trapping-detrapping process from bulk trap sites. Total D retention for specimen W53A (0.1 dpa, 673K) was >100 times larger than that of the unirradiated (0 dpa, 673K) specimen. D desorption from specimen W55A (0.1 dpa, 873K) also showed a similar wide desorption starting from 873K (plasma-exposure temperature) up to 1173K with the peak temperature around 1073K. D desorption from specimen W26A (0.1 dpa, 973K) also showed a similar desorption starting from 973K (plasma-exposure temperature) up to 1173K with the peak temperature around 1173K.

Figure 5 shows the total D retention from 0.1 dpa neutron-irradiated SCW and unirradiated (0 dpa) SCW. Total D retentions were calculated by integrating TDS spectra (D desorption flux) from room temperature (at t=0 s) to the end of 0.5 hr temperature hold (t~7200 s). Total D retention was approximately $1.9x10^{21}$ m^{-2} for specimen W53A (0.1 dpa, 673K). Considering the factor of 2 differences in ion fluence and the factor of 3 differences in displacement damage between the previous study [7] and this work, the D retention from W53A (0.1 dpa, 673K) sits close to the expected D retention for 673K from the previous study with PCW [7].

Table 2 summarizes the post irradiation examination (PIE) results from NRA and TDS for W53, W55, and W26 specimens. Near-surface D concentrations were obtained from the averaged NRA D depth profiles from the depth of 2.5 to 3.0 μm. The NRA D retentions were obtained by the integrating D/W from 0.0 μm to 3.0 μm. Atomic density of $6.3x10^{28}$ W/m^3 was used for the conversion from D/W to $D\text{-}m^{-2}$. Near-surface D concentrations were approximately $1.7x10^{-3}$, $1.5x10^{-4}$, and $4.9x10^{-5}$ D/W for W53B (673K), W55B (873K), and W26B (973K), respectively. The near-surface D concentration of $1.7x10^{-3}$ D/W from SCW (0.1 dpa, 673K) shows a reasonable agreement with our previous results of $4.0x10^{-3}$ D/W from PCW (0.3 dpa, 773K) considering the differences in plasma-exposure temperature (673K vs. 773K), damage dose (0.1 dpa vs. 0.3 dpa) and ion fluence ($5.0x10^{25}$ m^{-2} vs. $1.0x10^{26}$ m^{-2}) [6,7]. Detailed microstructure and defect analysis are required to understand the role of microstructure (e.g. single crystal vs. polycrystalline) in D retention. Although the near-surface D concentrations were decreased to $1.5x10^{-4}$ and $4.9x10^{-5}$ D/W at higher temperatures, the D atoms had migrated further and trapped in bulk trapping sites, resulting in non-negligible total D retention of $1.5x10^{20}$ and $1.2x10^{20}$ $D\text{-}m^{-2}$ for W55 (873K), and W26 (973K), respectively. The NRA near-surface D/W concentration averaged from the depth of 2.5 to 3.0 μm was used as the starting trap concentration in the TMAP modeling for neutron-induced trap concentration and to avoid the issue of detrapping of D atoms from the very near surface (<2.5 μm) trap sites during the cool-down after the plasma exposure at the higher temperature of 873 and 973K.

The ratio of the total D retention obtained by TDS to the near-surface D retention by NRA was approximately 5, indicating that D had diffused into the bulk neutron-irradiated tungsten specimen up to at least 15 μm (5x3 μm) during $7.1x10^3$ s plasma exposure for W53 (673K). Our previous study estimated that D atoms migrated and were trapped as far as 35 μm below the surface for 0.3 dpa at 773K [7]. The migration distance of 15 μm was in reasonable agreement with the previous estimate considering the differences in plasma-exposure temperature (673K vs. 773K), damage dose (0.1 dpa vs. 0.3 dpa) and ion fluence ($5.0x10^{25}$ m^{-2} vs. $1.0x10^{26}$ m^{-2}).

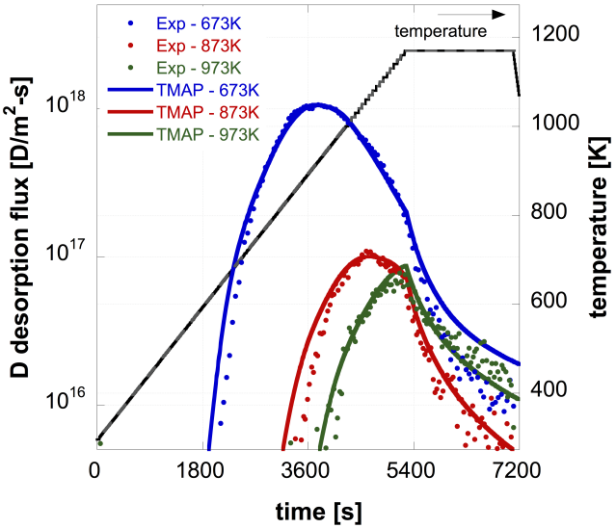

Figure 6: The experimental TDS spectrum (in dotted line) and the TMAP-simulated TDS spectrum (in solid line) of W53A (673K in blue), W55A (873K in red), and W26A (973K in green).

Table 3. The best-fit parameters obtained by fitting three experimental TDS spectra from 0.1 dpa HFIR neutron-irradiated tungsten specimens with TMAP.

TPE exposure temp. [K]	TMAP [a] trap conc. [Trap/W]	TMAP [b] detrapping energy [eV]	TMAP [b] binding energy [eV]	TMAP [c] reflection coefficient [N/D]
673	2.0E-3	1.80	1.41	0.90
873	2.0E-4	2.30	1.91	0.99
973	2.0E-4	2.60	2.21	0.99

[a] Uniform distribution of empty traps was introduced at the beginning of the simulation.

[b] The detrapping energy, E_{det}, is defined as the sum of the binding energy of D atom in trapping site, E_{bin}, and the activation energy of D diffusion in tungsten, E_d=0.39 eV.

[c] Integrated fraction of D atoms in the normal distribution (= 1 - reflection coefficient, R_{ref}) was adjusted to account for a complex plasma-surface interaction.

5. Modeling Results

Figure 6 shows the experimental and the TMAP-simulated TDS spectra of W53A (673K in blue), W55A (873K in red), and W26A (973K in green). Table 3 summarizes the best-fit parameters obtained by the TMAP modeling for three temperature cases. Three D desorption spectra were modeled with three fitting parameters: 1) trap concentration, n_{trap} [Trap/W], 2) detrapping energy, E_{det} [eV], and 3) reflection coefficient, R_{ref}. The experimental TDS are shown in dots, and the TMAP-simulated TDS spectra are plotted in sold lines. Although there was a little discrepancy in TDS spectra at beginning (673-773K), the TMAP was able to reproduce the experimental TDS spectrum well with (n_{trap} [Trap/W], E_{det} [eV], R_{ref}) = (2.0×10^{-3}, 1.80, 0.90) for W53A (0.1 dpa, 673K in blue). The TMAP obtained a trap concentration of 2.0×10^{-3} Trap/W, which is in good agreement with the near-surface D concentration of 1.7×10^{-3} D/W obtained from NRA. This is also in reasonable agreement with the near-surface D concentration of 4.0×10^{-3} D/W and the detrapping energy of 1.80 eV that Hatano *et al.* obtained from 0.3 dpa neutron-irradiated PCW exposed at 773K [6]. A reasonable agreement between the experimental TDS and the TMAP-simulated spectra were also obtained for 873K and 973K cases. The TMAP trap concentration of 2.0×10^{-4} T/W is in good agreement with the near-surface D concentration of 1.5×10^{-4} D/W obtained from NRA for 873K case, but there was a factor of 4 difference between the TMAP trap concentration of 2.0×10^{-4} Trap/W and the near-surface D concentration of 4.9×10^{-5} D/W obtained from NRA for 973K case. This difference is due to detrapping of D atoms from the near surface trap sites during the cool-down after the plasma exposure at the higher temperature. In addition, large detrapping energies of 2.30 and 2.60 eV were required to fit the experimental TDS spectra for 873K and 973K, respectively. From the literature of the detrapping energy in tungsten [26-29], the low-energy (E_{bin} = 0.4-0.8 eV) trap is associated with D atoms trapped in impurities or dislocations, the medium-energy (E_{bin} = 0.8-1.4 eV) trap is associated with D atoms trapped at vacancies in tungsten and D_2 molecules desorbed from voids, and the high-energy (E_{bin} = 1.4-2.2 eV) trap is associated with dissociation and release of D atoms decorating a large vacancy cluster or void. One of possible mechanism(s) for the higher detrapping energy trap sites is due to defects annealing at elevated temperature and formation of higher detrapping energy trap sites. In addition, one of the candidate mechanism(s) for the factor of 10 differences in TMAP trap concentration between 673K and 873-973K is due to the defect annealing at higher temperature (873-973K).

6. Discussion

Neutrons produce radiation damage and lattice defects such as vacancies, vacancy-clusters, voids, dislocations, and dislocation loops in tungsten. High-flux D plasmas also create near-surface damage such as D precipitations and blisters. Uncovering D/T trapping mechanisms requires an understanding of microstructural evolution of the radiation defects, defect annealing at elevated temperature, and defect interaction with diffusing D/T atoms and solid transmutation atoms (e.g. tantalum, rhenium, osmium in tungsten) in bulk material as well as effects of plasma-induced near-surface defects.

Figure 2 and 4 show that large D retention was observed from the 0.1 dpa neutron-irradiated SCW without visibly large (> 5 μm) blister formations, indicating that the visibly large blisters may not play a major role in D retention in these neutron-irradiated SCW specimens for the tested incident ion energies and ion flux densities. Relatively large blisters (> 5 μm) were visible in low dose (0.025 dpa) neutron-irradiated PCW exposed to similar D plasma conditions [30]. The reduction of blister formation might be due to the crystal orientation and/or the use of rough and technical surfaces of the SCW specimens [11,12]. Ratios of the total D retention obtained by TDS and the near-surface D retention by NRA were more than 5 for the 0.1 dpa neutron-irradiated SCW exposed at the temperature above 673K, indicating plasma-induced near-surface defects do not play a critical role in D/T retention in neutron-irradiated SCW exposed at elevated temperature.

Detailed microstructural and defect characterization of SCW irradiated at similar irradiation dose and temperature is not yet available. Hu *et al.*, however, performed positron annihilation spectroscopy and transmission electron microscopy studies on low-temperature (~363K) and low-dose (0.006 and 0.03 dpa) neutron-irradiated SCW during isochronal annealing [31]. The defect size and density were obtained by fitting positron lifetime spectra with 200, 375, and 500 ps lifetimes, equivalent to three-dimensional vacancy clusters of approximate size of 0.31, 0.67 and >1.00 nm in diameter, respectively. The significant increase in small vacancy clusters density was observed after low temperature neutron-irradiation in the HFIR. The growth of intermediate-size (0.67 nm) and large vacancy clusters (>1.00 nm) and the reduction of the small

vacancy cluster (0.31 nm) density were observed in 0.03 dpa neutron-irradiated SCW after isochronal annealing at 673K for 1 hr. It was also observed that intermediate-size and large vacancy clusters were relatively stable in the temperatures from 923K to 1273 K. The densities of intermediate-size and large vacancy clusters were only decreased after annealing above 1273K. According to the observations by Hu *et al.* and this work [7, 31], the HFIR neutrons produce predominantly small vacancy clusters (including vacancies and di-vacancies) at low irradiation temperature, creating medium-energy (E_{bin} = 0.8-1.4 eV) trapping sites for D/T atoms in tungsten. As the neutron irradiation and/or plasma exposure temperature go above the stage III recovery (defect recovery due to vacancy migration) temperature of 623-673K, agglomerations of the small vacancy clusters form the intermediate-size and large vacancy clusters, generating high-energy (E_{bin} = 1.4-2.2 eV) trapping sites for D/T atoms in tungsten [7, 31, 32]. The intermediate-size and large vacancy clusters remained as trapping sites for diffusing D/T atoms even at elevated temperature of 873K and 973K. If this is true, non-negligible concentration of high-energy trapping sites should remain in the SCW specimen exposed at elevated temperature of 873K and 973K. In this study, the TMAP model suggested that a non-negligible concentration (2.0×10^{-4} [Trap/W]) of high-energy traps (E_{bin} = 1.9 and 2.2 eV) exists in the SCW specimen exposed to elevated temperature of 873K (W55) and 973K (W26). The NRA near-surface D concentration and TMAP trap concentration were similar for W53 (673K) and W55 (873K), indicating that near-surface traps were saturated with D atoms at the temperature from 673K to 873K. The difference between the NRA near-surface D concentration and the TMAP trap concentrations for 973K (W26) was because the near-surface traps were not saturated with D atoms at the temperature of 973K. Large detrapping energies of 2.30 and 2.60 eV were required to fit the experimental TDS spectra for W55 (873K) and W26 (973K), respectively. Extensive microstructure and defect analysis are required to reveal the defect types of the high detrapping energy traps in neutron-irradiated tungsten.

7. Concluding Remarks

Six SCW specimens were irradiated to create radiation damage of 0.1 dpa at three different irradiation temperatures (633K, 963K, and 1073K) in the HFIR at ORNL. A pair of neutron-irradiated SCW specimens was exposed to D plasma to D ion fluence of 5.0×10^{25} m^{-2} at three different exposure temperatures (673K, 873K, and 973K) in the TPE at INL. A broad D desorption spectrum from plasma-exposure temperature up to 1173K was observed. Total D retention up to 1.9×10^{21} m^{-2} and near-surface D concentration up to 1.7×10^{-3} D/W were experimentally measured from the 0.1 dpa neutron-irradiated SCW. Trap density up to 2.0×10^{-3} Trap/W and the high detrapping energy ranging from 1.80 to 2.60 eV were obtained from the TMAP modeling. The D retention in the 0.1 dpa neutron-irradiated SCW decreased with increasing temperature. One of the candidate mechanisms is due to the annealing of defects above 673 K and the incomplete filling (i.e. dynamical detrapping) at elevated plasma exposure temperature. Comprehensive microstructure and defect analysis are necessary to uncover the defect types of the high detrapping energy traps in neutron-irradiated tungsten.

Acknowledgments

This work was prepared for the U. S. Department of Energy, Office of Fusion Energy Sciences, under the DOE Idaho Field Office contract number DE-AC07-05ID14517 and the DOE National Nuclear Security Administration contract number DE-AC04-94AL85000.

References

[1] N. Taylor, C. Alejaldre, and P. Cortes, Progress in the safety and licensing of ITER, *Fus. Sci. Technol.* **64** (2013) 111-117.

[2] N. Taylor, B. Merrill, L. Cadwallader, L. di Pace, L. El-Guebaly, P. Humrickhouse, D. Pnayotov, T. Pinna, M.T. Porfiri, S. Reyes, M. Shimada, and S.R. Willms, Materials-related issues in the safety and licensing of nuclear fusion facilities, *Nucl. Fusion* **57** (2017) 092003.

[3] Y. Ueda, J.W. Coenen, G. De Temmerman, R.P. Doerner, J. Linke, V. Philipps, and E. Tsitrone, Research status and issues of tungsten plasma facing materials for ITER and beyond, *Fus. Eng. Des.* **89** (2014) 901.

[4] Y. Oya, M. Shimada, T. Oda, M. Hara, Y. Hatano, P. Calderoni, and K. Okuno, Comparison of deuterium retention for ion-irradiated and neutron-irradiated tungsten, *Phys. Scr.*, **T145** (2011) 014050.

[5] Y. Hatano, M. Shimada, V.Kh. Alimov, J. Shi, M. Hara, T. Nozaki, Y. Oya, M. Kobayashi, K. Okuno, T. Oda, G. Cao, N. Yoshida, N. Futagami, K. Sugiyama, J. Roth, B. Tyburska-Püschel, J. Dorner, I. Takagi, M. Hatakeyama, H. Kurishita, and M.A. Sokolov, Trapping of hydrogen isotopes in radiation defects formed in tungsten by neutron and ion irradiations, *J. Nucl. Mater.* **438** (2013) S114.

[6] Y. Hatano, M. Shimada, T. Otsuka, Y. Oya, V.Kh. Alimov, M. Hara, J. Shi, M. Kobayashi, T. Oda, G. Cao, K. Okuno, T. Tanaka, K. Sugiyama, J. Roth, B. Tyburska-Püschel, J. Dorner, N. Yoshida, N. Futagami, H. Watanabe, M. Hatakeyama, H. Kurishita, M.A. Sokolov, and Y. Katoh, Deuterium trapping at defects created with neutron and ion irradiations in tungsten, *Nucl. Fusion* **53** (2013) 073006.

[7] M. Shimada, G. Cao, T. Otsuka, M. Hara, M. Kobayashi, Y. Oya, and Y. Hatano, Irradiation effect on deuterium behaviour in low-dose HFIR neutron-irradiated tungsten, *Nucl. Fusion* **55** (2015) 013008.

[8] Y. Katoh, D. Clark, Y. Ueda, Y. Hatano, M. Yoda, A. S. Sabau, T. Yokomine, L. M. Garrison, W. Geringer, A. Hasegawa, T. Hinoki, M. Shimada, D.A. Buchenauer, Y. Oya, and T. Muroga, Progress in the U.S./Japan PHENIX project for the technological assessment of plasma racing components for DEMO reactors, *Fus. Sci. Technol.* **72** (2017) 222.

[9] M. Shimada, Y. Oya, D.A. Buchenauer, and Y. Hatano,

Hydrogen isotope retention and permeation in neutron-irradiated tungsten and tungsten alloys under PHENIX collaboration, *Fus. Sci. Technol.* **72** (2017) 652.

[10] B. Lipschultz *et al.*, An assessment of the current data affecting tritium retention and its use to project towards T retention in ITER, MIT Report PSFC/RR-10–4 (2010).

[11] A. Manhard, M. Balden, and U. von Toussaint, Blister formation on rough and technical tungsten surfaces exposed to deuterium plasma, *Nucl. Fusion* **57** (2017) 126012.

[12] D. Nishijima, H. Iwakiri, K. Amano, M.Y. Ye, N. Ohno, K. Tokunaga, N. Yoshida and S. Takamura, Suppression of blister formation and deuterium retention on tungsten surface due to mechanical polishing and helium pre-exposure, *Nucl. Fusion* **45** (2005) 669.

[13] R.L. Greenwood, K.R. Smither, SPECTER: Neutron Damage Calculations for Materials Irradiations, 1985. ANL/FPP/TM-197.

[14] M. Shimada, R.D. Kolasinski, R.A. Causey, J.P. Sharpe, Tritium Plasma Experiment: Parameters and Potentials for Fusion Plasma-Wall Interaction Studies, *Rev. Sci. Instr.*, **82** (2011) 083503.

[15] M. Shimada, C.N. Taylor, L. Moore-McAteer, R.J. Pawelko, R.D. Kolasinski, D.A. Buchenauer, L.C. Cadwallader, and B.J. Merrill, TPE upgrade for enhancing operational safety and improving in-vessel tritium inventory assessment in fusion nuclear environment, *Fusion Engineering and Design*, **109-111** (2016) 1077.

[16] M. Shimada, C.N. Taylor, R.J. Pawelko, L.C. Cadwallader, and B.J. Merrill, Tritium Plasma Experiment Upgrade and Improvement of Surface Diagnostic Capabilities at STAR Facility for Enhancing Tritium and Nuclear PMI Sciences, *Fusion Science and Technology* **71** (2017) 310.

[17] W.R.Wampler, D.L.Rudakov, J.G.Watkins, and C.J.Lasnier, The influence of displacement damage on deuterium retention in tungsten exposed to divertor plasma in DIII-D, *J. Nucl. Mater.* **415** (2011) S653.

[18] M. Mayer, *SIMNRA User's Guide*, Technical Report, IPP 9/113 Garching (1997) <http://www.rzg.mpg.de/~mam>.

[19] G.R. Longhurst, D.F. Holland, J.L. Jones, and B.J. Merrill, *TMAP4 User's Manual*, Idaho National Laboratory, EGG-FSP-10315 (1992).

[20] B.J. Merrill, M. Shimada, and P.W. Humrickhouse, Simulating tritium retention in tungsten with a multiple trap model in the TMAP code, *J. Plasm. Fus. Res. SERIES*, **10** (2013) 71.

[21] B.J. Merrill, P.W. Humrickhouse, and M. Shimada, Recent development and application of a new safety analysis code for fusion reactors, *Fus. Eng. Des.* **109-111** (2016) 970.

[22] R. Frauenfelder, Solution and diffusion of hydrogen in tungsten, *J. Vac. Sci. Technol.* **6** (1969) 388.

[23] R.A. Causey, Hydrogen isotope retention and recycling in fusion reactor plasma-facing components, *J. Nucl. Mater.* **300** (2002) 91.

[24] Stopping and Range of Ions in Matter (SRIM), J.F. Ziegler, http://www.srim.org

[25] R.D. Kolasinski, D.F. Cowgill, D.C. Donovan, M. Shimada, and W.R. Wampler, Mechanisms of gas precipitation in plasma-exposed tungsten, *J. Nucl. Mater.* **438** (2013) S1019.

[26] O.V. Ogorodnikova, J. Roth, and M. Mayer, Ion-driven deuterium retention in tungsten, *J. Appl. Phys.* **103** (2008) 034902.

[27] O.V. Ogorodnikova, Fundamental aspects of deuterium retention in tungsten at high flux plasma exposure, *J. Appl. Phys.* **118** (2015) 074902.

[28] H. Eleveld, and A. van Veen, Deuterium interaction with impurities in tungsten studied with TDS, *J. Nucl. Mater.* **191-194** (1992) 433.

[29] H. Eleveld H, and A. van Veen, Void growth and thermal desorption of deuterium from voids in tungsten, *J. Nucl. Mater.* **212-215** (1994) 1421.

[30] M. Shimada, G Cao, Y Hatano, T Oda, Y Oya, M Hara and P Calderoni, The deuterium depth profile in neutron-irradiated tungsten exposed to plasma, *Phys. Scr.* **T145** (2011) 014051.

[31] X. Hu, T. Koyanagi, M. Fukuda, Y. Katoh, L.L. Snead, and B.D. Wirth, Defect evolution in single crystalline tungsten following low temperature and low dose neutron irradiation, *J. Nucl. Mater.* **470** (2016) 278.

[32] H. Schultz, *The Landolt–Bornstein Database* volume III/25 (www.springermaterials.com) *Atomic Defects in Metals* (*Springer Materials*) ed H. Ullmaier, section 2.2.3 (1991) doi:10.1007/10011948 54